Trans Indian Inst Met (2016) 69(3):805–815
DOI 10.1007/s12666-015-0556-2

TECHNICAL PAPER

Sulfur Containing Compounds as Corrosion Inhibitors for Mild Steel in Hydrochloric Acid Solution

Hojat Jafari[1] · **Koray Sayin**[2]

Received: 24 December 2014 / Accepted: 1 May 2015 / Published online: 9 June 2015

Abstract The role of Sulfur containing compounds namely: Thiobarbituric acid (TBA) and Thiourea (TH) as corrosion inhibitors for mild steel in 1 M HCl has been studied using potentiodynamic anodic polarization, electrochemical impedance spectroscopy, atomic force microscopy and scanning electron microscopy techniques. Polarization results showed that all the compounds studied are mixed type inhibitors. Electrochemical impedance studies showed that the presence of these compounds decreases the double-layer capacitance and increases the charge transfer resistance. Quantum chemical calculation was further applied to reveal the adsorption structure and explain the experimental results. The results of calculations showed superior inhibition efficiency of TH in comparison to TBA.

Keywords Acid solutions · Steel · Electrochemical calculation · SEM · AFM · Quantum chemical calculation

1 Introduction

Most large structures in industries are made by mild steel owing to it's low-cost, availability and strength. But it is also highly susceptible to corrosion, especially in acidic media [1]. Acid solutions are frequently used for the removal of rust and scale in several industrial processes, which causes corrosion damage to equipment and pipeline systems made of steel [2]. The most commonly used acids are hydrochloric, sulfuric, nitric, hydrofluoric, citric, formic, and acetic acid [3].

The use of inhibitors is one of the most practical methods for protection against corrosion, especially in acidic media. Many studies have been made on the corrosion and inhibition of steels in acid media [4–11]. Among numerous inhibitors that have been tested and applied industrially as corrosion inhibitors, those that are nontoxic or of low toxicity are now far more strategic than in the recent past. In the twenty-first century, research in the field of green or eco-friendly corrosion inhibitors have been addressed toward the goal of using cheap, efficacious compounds of ignorable or "zero" environmental impact. Organic compounds bearing heteroatoms with high electron density such as phosphor, sulphur, nitrogen, oxygen or those containing multiple bonds which are considered as adsorption centers, are effective as corrosion inhibitors [12–14]. The compounds containing both nitrogen and sulphur in their molecular structure have exhibited greater inhibition compared with those containing only one of these atoms [15–17].

The correlation between the structures and corrosion inhibition efficiencies of thio acetamide (TACA), thiourea (TH) and thiobenzamide (TBA) on the corrosion of mild steel in 0.1 M H_2SO_4 solution have been investigated using quantum chemical calculations by Ozcan et al. [18]. It was seen that there is a clear relation between the increase in corrosion inhibition and the increase of the highest occupied molecular orbital (HOMO) energy level. Saxena et al. [19] investigated the corrosion inhibition performance of mild steel in nitric acid solution containing different concentration of Schiff bases. Sastri [4] studied the effect of

✉ Hojat Jafari
hojatjafari80@yahoo.com

[1] Abadan Faculty of Petroleum Engineering, Petroleum University of Technology, Abadan, Iran

[2] Department of Chemistry, Institute of Science, Cumhuriyet University, 58140 Sivas, Turkey

some amino pyrimidine derivatives on the corrosion of carbon steel in 0.05 M HCl solution. The results revealed that these inhibitors acted as mixed type inhibitors and their inhibition was due to the adsorption of their molecules on the steel surface.

The purpose of this paper is to compare the corrosion inhibition data obtained from Tafel extrapolation, EIS, SEM and AFM techniques for TH with that obtained for TBA. Furthermore, theoretical calculations have been performed by the density functional theory (DFT) to understand the mechanism of adsorption of these inhibitors.

2 Experimental

2.1 Materials

The working electrode was a cylindrical disc cut from a steel rod with the following chemical compositions (%w); 0.21 C, 0.035 Si, 0.25 Mn, 0.082 P, and Fe (remainder). The mild steel specimen was coated with polyester block, aspect for measurement and the electrical conductivity was provided by a copper wire. The steel plate of cylindrical shape was encapsulated in Teflon in such a way that only one surface was left uncovered. The exposed area (0.32 cm^2) was mechanically abraded with a series of Emery papers of variable grades, starting with a coarse one and proceeding in steps to the finest (1200) grade.

The aggressive solution of 1 M HCl was prepared by dilution of Merck Product HCl. The concentration range of inhibitors employed was 4×10^{-4} and 6×10^{-3} M. All chemicals used in present work were of reagent-grade Merck product and used as received without further purification. The inhibitors used were Thiourea (TH) N_2H_4CS and Thiobarbituric acid (TBA) $C_4H_4N_2O_2S$ (Fig. 1).

2.2 Methods

The apparatus for electrochemical investigations consists of a computer-controlled Auto Lab potentiostat/galvanostat (PGSTAT302 N) corrosion measurement system at a scan rate of $1mVs^{-1}$. The experiments were carried out using a conventional three electrode cell assembly at 25 ± 2 °C. A rectangular platinum foil was used as counter electrode and saturated calomel electrode as the reference electrode. Time interval of 20–25 mins was given for steady-state attainment of open circuit potential.

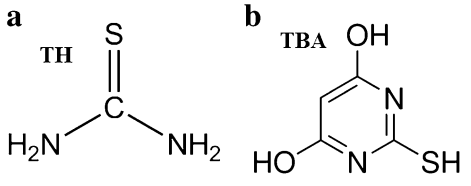

Fig. 1 The chemical structure of the inhibitors: **a** TH, **b** TBA

For surface analysis, the specimens of size 0.32 cm^2 were abraded with Emery paper (up to 1200) to give a homogeneous surface, then washed with distilled water and acetone. The specimens were immersed in 1 M HCl prepared with and without addition of 6×10^{-3} M of the inhibitor at 25 ± 2 °C for 6 h and cleaned with distilled water. The surface morphology of the electrode surface was evaluated by atomic force microscopy (AFM) Nan Surf easyscan2 and scanning electron microscopy (VEGA).

Construction drawings and displaying were done by using GaussView 5.0.8 [20] and all calculations were performed by using Gaussian 09 AM64L-G09RevC.01 package program [21]. Additionally, preparation of figures was done by using ChemBioDraw Ultra Version (13.0.0.3015) [22]. M062X hybrid function [23] which is one of the density functional theories was selected as a computational method for investigating inhibitors. In calculations, 6-311++G (d, p) was selected as the basis set. All calculations were performed in gas phase and additionally optimized structures for non-protonated inhibitors were re-calculated in water. The vibration frequency analyses indicated that optimized structures of all inhibitors were at stationary points corresponding to local minima without imaginary frequencies. The interactions of solute–solvent were taken into account by the conductor-like polarizable continuum model (CPCM). Some quantum chemical descriptors were calculated by using Eqs. (1)–(11) [24–31].

$$E_{GAP} = E_{LUMO} - E_{HOMO} \tag{1}$$

$$I = E_{Total}(N) - E_{Total}(N-1) \tag{2}$$

$$A = E_{Total}(N+1) - E_{Total}(N) \tag{3}$$

$$\eta = \frac{|I - A|}{2} \tag{4}$$

$$\sigma = \frac{1}{\eta} \tag{5}$$

$$\chi = \frac{|E_{HOMO} + E_{LUMO}|}{2} \tag{6}$$

$$\mu = -\chi \tag{7}$$

$$\omega = \frac{\mu^2}{2\eta} \tag{8}$$

$$N = \frac{1}{\omega} \tag{9}$$

$$PA = E_{Pro.} - (E_{Non-pro.} + E_{H^+}) \tag{10}$$

$$E_{H^+} = E_{H_3O^+} - E_{H_2O} \tag{11}$$

Where E_{HOMO} and E_{LUMO} are the energy of the Frontier molecular orbital HOMO and LUMO. The ionization

potential (I), the electron affinity (A), electronegativity (χ), chemical potential (μ), hardness (η), softness (σ), electrophilicity index (ω) and Nucleophilicity index (N) are given by Eqs. (2)–(9). $E_{\text{Total}}(N)$, $E_{\text{Total}}(N-1)$ and $E_{\text{Total}}(N+1)$ mean total energy of the (N)-electron systems, total energy of the $(N-1)$-electron systems and total energy of the $(N+1)$-electron systems respectively. $E_{\text{non-pro.}}$, $E_{\text{pro.}}$ and E_{H+} are energy of non-protonated inhibitors, protonated inhibitors and H^+ ion, respectively.

3 Results and Discussion

3.1 Electrochemical Results

Figures 2 and 3 show the representative Tafel polarization curves of steel in 1 M HCl solution in the presence of

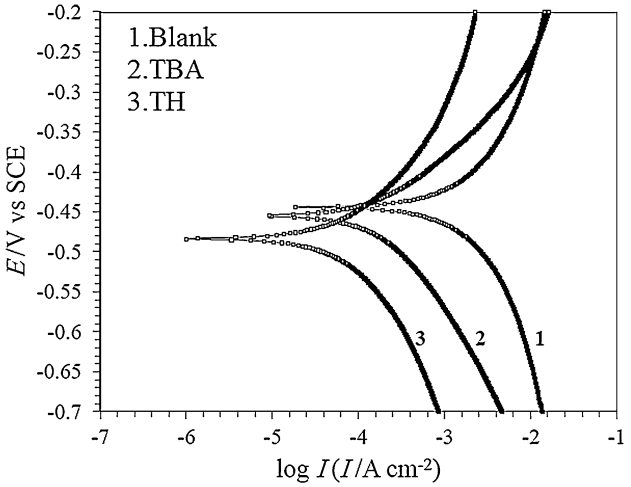

Fig. 2 Tafel polarization curves for steel in the 1 M HCl (**1**), in the presence of 4×10^{-4} M of TBA (**2**), TH (**3**)

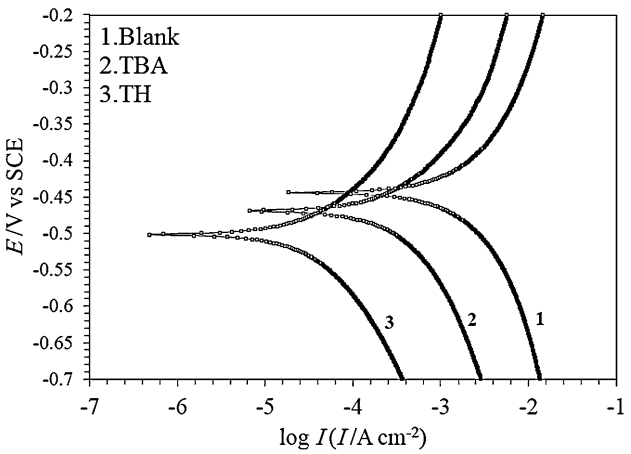

Fig. 3 Tafel polarization curves for steel in the1 M HCl (**1**), in the presence of 6×10^{-3} M of TBA (**2**), TH (**3**)

4×10^{-4} M and 6×10^{-3} of TH and TBA. Similar data were also obtained in the presence of other concentrations, which are not brought here for summary.

The corresponding electrochemical parameters, i.e., corrosion potential (E_{corr} vs. SCE), corrosion current density (I_{corr}), cathodic and anodic Tafel slopes (β_a, β_c) and the degree of surface coverage (θ) values were calculated from these curves and are given in Table 1. The degree of surface coverage for different concentrations of inhibitors is calculated using the following equations [32]:

$$\theta = \frac{I - \dot{I}}{I} \tag{12}$$

Where I and $\dot{I}$ are the corrosion current densities without and with corrosion inhibitor, respectively, determined by the intersection of the extrapolated Tafel lines at the corrosion potential for steel in uninhibited and inhibited acid solution.

The presence of inhibitors shifts both anodic and cathodic branches to the lower values of corrosion current densities and thus causes a remark able decrease in the corrosion rate (Figs. 2, 3). It can be clearly seen from Figs. 2 and 3 that, as would be expected, both anodic metal dissolution of iron and cathodic hydrogen evolution reactions were inhibited after the addition of inhibitor to the aggressive solution. This result is indicative of the adsorption of inhibitor molecules on the active sites of steel surface [20]. The inhibition of both anodic and cathodic reactions is more pronounced with the increasing inhibitor concentration. However, the influence is more pronounced in the cathodic polarization plots compared to that of the anodic polarization plots.

The cathodic current–potential curves giving rise to parallel lines indicates that the addition of inhibitors to the 1 M HCl solution does not modify the reduction mechanism and the reduction at steel surface takes place mainly through a charge transfer mechanism [33, 34]. The corrosion potential displayed small change versus SCE and curves changed slightly towards the negative direction (Figs. 2, 3) indicating an adsorption to protect steel, consequently these compounds can be classified as mixed corrosion inhibitors, as electrode potential displacement is lower than 85 mV in any direction [35].

By increasing the inhibitor concentration, the polarization resistance increases in the presence of compound, indicating adsorption of the inhibitor on the metal surface to block the active sites efficiently and inhibit corrosion [35]. Figures 2 and 3 show that the lower corrosion current was obtained for TH and therefore, TH is more beneficial rather than TBA. The best inhibition efficiency was about 99 % at concentration 6×10^{-3} M for TH.

Figures 4 and 5 shows the Nyquist diagrams of steel in 1 M HCl solution containing different concentrations of TH and TBA at E_{corr}. The plots show a depressed capacitive loop

Table 1 Potentiodynamic polarization parameters for the corrosion of Mild steel in 1M HCL solution in absence and presence of different concentrations of inhibitors

Inhibitor	Concentration/M	−Ecorr/mV	Icorr/μA cm^{-2}	βa/mVdec^{-1}	−βc/mVdec^{-1}	θ	IE %
	Blank	444	794	159	215	–	–
TH	4×10^{-1}	484	50	64	202	0.93	93
	6×10^{-3}	503	13	61	110	0.98	98
TBA	4×10^{-4}	475	251	75	134	0.68	68
	6×10^{-3}	479	79	69	132	0.83	83

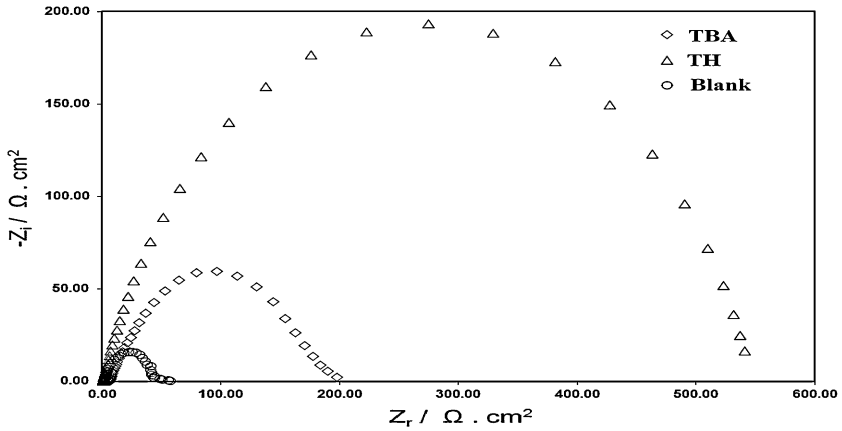

Fig. 4 EIS spectra of carbon steel for the blank test and inhibition test at the concentration of 4×10^{-4} M in 1 M HCl in the presence of TBA and TH

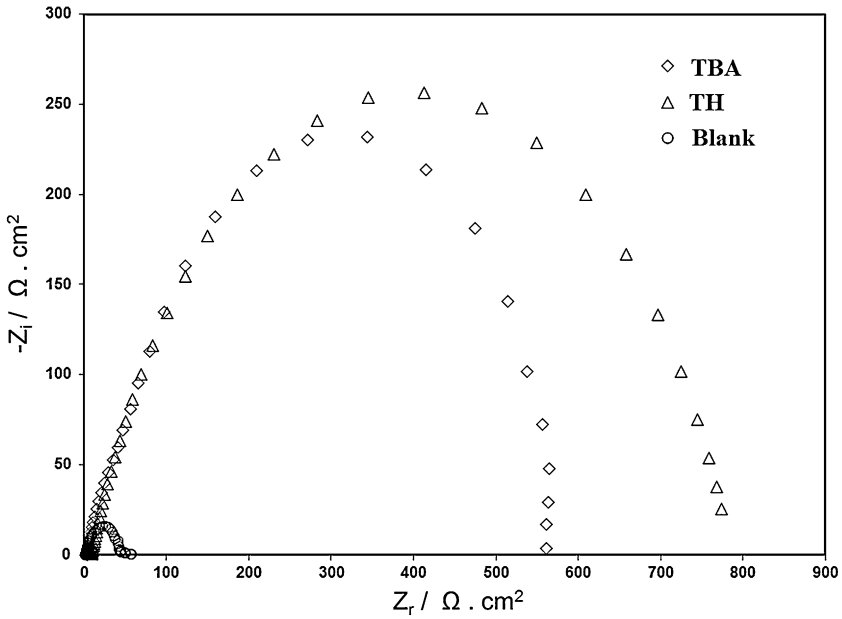

Fig. 5 EIS spectra of carbon steel for the blank test and inhibition test at the concentration of 6×10^{-3} M in 1 M HCl in the presence of TBA and TH

which arises from the time constant of the electrical double layer, and charge transfer resistance. As it can be seen, higher charge transfer resistance was obtained in presence of TH.

The impedance of the inhibited steel increases with increasing concentration of inhibitors and consequently, the inhibition efficiency increases. The equivalent circuit compatible with the Nyquist diagram recorded in the presence of inhibitors is depicted in Fig. 6a.

To obtain a satisfactory impedance simulation of steel, it is necessary to replace the capacitor (C) with a constant phase element (CPE) Q in the equivalent circuit. The most widely accepted explanation for the presence of CPE behavior and depressed semicircles on solid electrodes is microscopic roughness, causing an inhomogeneous distribution in the solution resistance as well as in the double-layer capacitance [36].

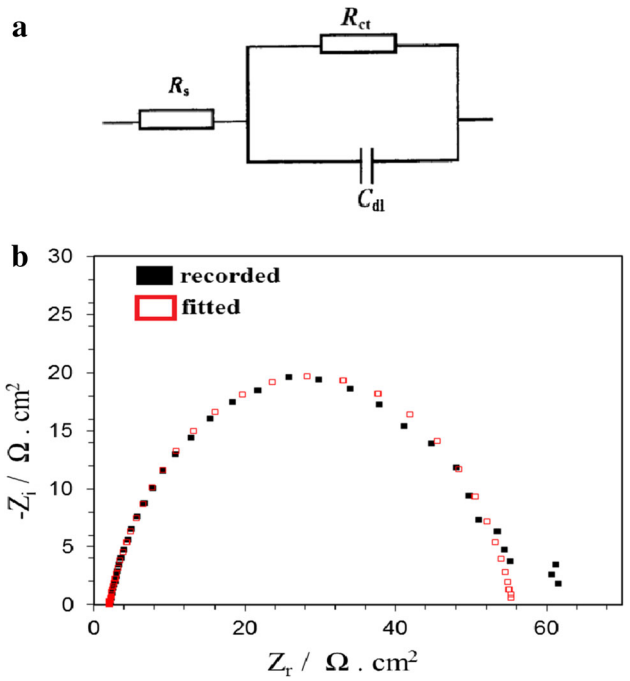

Fig. 6 **a** Equivalent circuits compatible with the experimental impedance data in Figs 4 and 5 for corrosion of steel electrode in 1 M hydrochloric acid solution. **b** Experimental and computer fit result of Nyquist plot for steel in 1 M HCl at 25 °C

Constant phase element Q_{dl}, R_s and R_{ct} can be corresponded to double layer capacitance, solution resistance, and charge transfer resistance respectively. To corroborate the equivalent circuit, the experimental data are fitted to the equivalent circuit, and the circuit elements are obtained.

The equivalent circuit compatible with the Nyquist diagram recorded in the absence of inhibitor is depicted in Fig. 6b. Table 2 illustrates the equivalent circuit parameters for the impedance spectra of corrosion of steel in 1 M HCl solution. The results demonstrate that the presence of inhibitors enhanced the value of R_{ct} obtained in the pure medium while that of Q_{dl} is reduced. The decrease in Q_{dl} values was caused by adsorption of inhibitor indicating that the exposed area got decreased. On the other hand, a decrease in Q_{dl}, which can result from a decrease in local dielectric constant and/or an increase in the thickness of the electrical double layer, suggests that inhibitors act by adsorption at the metal–solution interface.

As the Q_{dl} exponent (n) is a measure of the surface heterogeneity, values of n indicates that the steel surface becomes more and more homogeneous as the concentration of inhibitor increases as a result of its adsorption on the steel surface and corrosion inhibition. The increase in values of R_{ct} and the decrease in values of Q_{dl} with increase in the concentration also indicate that inhibitors act as primary interface inhibitors and the charge transfer controls the corrosion of steel under the open- circuit conditions.

3.2 Molecular Structure and Quantum Chemical Calculation

3.2.1 Non-Protonated Inhibitors

Both inhibitors are optimized at M062X/6-311++G (d, p) level and optimized structures of inhibitors are represented in Fig. 7. Quantum chemical descriptors are calculated for non-protonated TH and TBA and are listed in Table 3.

E_{HOMO} is a quantum chemical descriptor/parameter and mainly associated with electron donating ability of molecules. High value of E_{HOMO} implies the tendency of electron transfer to a low empty molecular orbital of appropriate acceptor molecule. The low E_{LUMO} value indicates that the electron accepting ability of the molecule is higher [31]. If the E_{HOMO} and E_{LUMO} are decisive for investigated inhibitors, the ranking of the compounds should be:

$$\text{TH} > \text{TBA} \ (\text{according to } E_{HOMO} \text{ and } E_{LUMO})$$

The E_{GAP} is a significant parameter as a function of activity of the corrosion inhibitors towards the metal surface. The smaller E_{GAP} values mean the more activity and higher inhibition efficiency. According to E_{GAP} values, the ranking of inhibition efficiency should be as follows:

$$\text{TH} > \text{TBA} \ (\text{according to } E_{GAP})$$

Other important parameters are hardness (η) and softness (σ) to explain the inhibitors efficiencies. Tendencies of electron transferring of inhibitors towards the metal atom or metallic bulk can be discussed with hard-soft-acid–base (HSAB) approximation [30]. According to this approximation, hard/soft chemical species prefer to

Table 2 Impedance data for steel in 1 M HCl solution without and with different concentrations of inhibitors at 25 °C

Inhibitor	Concentration/M	R_s/Ω cm^2	R_{ct}/Ω cm^2	Q_{dl}/mF cm^2	C_{dl}/mF cm^2	n
	Blank	1.6	56	0.683	0.210	0.74
TH	4×10^{-4}	1.7	541	0.138	0.061	0.76
	6×10^{-3}	1.4	770	0.105	0.052	0.78
TBA	4×10^{-4}	1.8	186	0.253	0.091	0.75
	6×10^{-3}	1.2	568	0.180	0.075	0.76

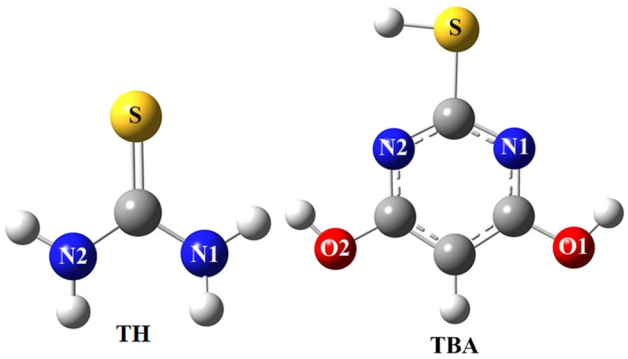

Fig. 7 Optimized structures of TU and TBA at M062X/6-311++G(d,p) level in gas phase

coordinate to hard/soft species. As a result, soft species are to be most effective for metallic bulks. Because metallic bulk is softer than metal atoms [37]. According to softness values, inhibition efficiency ranking should be:

TH > TBA (according to softness)

Another important parameter is global electronegativity. The absolute electronegativity is related with freedom of electron mobility in molecule. The small electronegativity means that electrons in inhibitors are freer than others. Corrosion inhibitors coordinate to the metal surface by giving electrons. The inhibition efficiency, therefore, increases with decreasing of absolute electronegativity values. According to this parameter, inhibition efficiency ranking should be as follow:

TH > TBA (according to absolute electronegativity)

The other important parameters are ω and *N*. The electrophilicity index (ω) implies the ability of the inhibitor molecules to accept electrons. Nucleophilicity index (*N*) displays the ability of inhibitors to donate electrons. The inhibition efficiency increases with increasing the N value or decreasing the ω value. According to the N and ω, theoretical inhibition efficiency ranking should be:

TH > TBA (according to electrophilicity and nucleophilicity ii

All rankings are appropriate with their experimental results.

3.2.2 *Determination of Active Site*

Active site of TH is only sulphur atom. Since, there are three bonds around the nitrogen atoms while for sulphur atom its octet is not completed. As for the TBA, there are three different heteroatoms which are oxygen, nitrogen and sulphur atoms. Proton affinity (PA) of each heteroatom in TBA are calculated as 180.517, 193.686, 342.734, 346.538, 305.237 kJ mol^{-1} for N1, N2, O1, O2 and S atom in TBA molecule, respectively. The lower PA values mean stronger proton acceptor. Therefore, N1 atom in TBA is an active site for corrosion. Contour diagram of HOMO for each inhibitor are calculated and represented in Fig. 8.

According to Fig. 8, sulphur atom in TH is an active site because HOMO electrons are mainly localized on sulphur atom. As for the HOMO of TBA, electrons are localized on whole molecule. It is therefore difficult to say active site for TBA. As a result, S atom in TH molecule and N1 atom in TBA molecule are active sites for our inhibitors.

3.2.3 *Molecular Electrostatic Potential (MEP) Map and Contour*

Molecular electrostatic potential (MEP) map are contoured and related to electron density on the inhibitor surface. MEP maps and contours of investigated inhibitors are

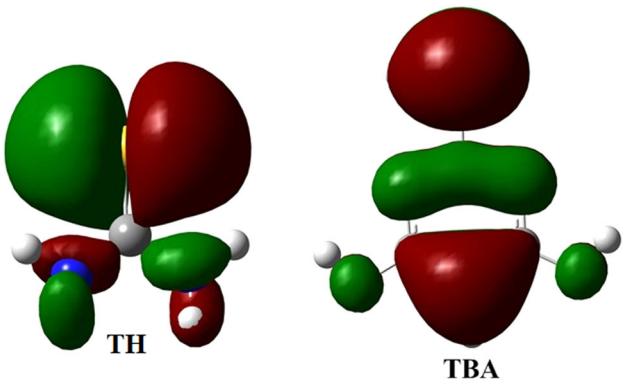

Fig. 8 Contour diagrams of HOMO in TU and TBA molecules at M062X method with 6-311++G(d,p) basis set

Table 3 Quantum chemical descriptors for non-protonated inhibitors at M062X/6-311 ++G(d,p) level in gas phase

Inhibitor	E_{HOMO} (eV)	E_{LUMO} (eV)	E_{GAP} (eV)	I (eV)	A (eV)
TU	−7.259	−0.579	6.680	−0.372	8.282
TBA	−8.188	−0.159	8.029	−0.775	8.987
Inhibitor	η (eV)	σ (eV^{-1})	χ (eV)	ω (eV)	N (eV^{-1})
TU	4.327	0.231	3.919	1.775	0.563
TBA	4.881	0.205	4.174	1.784	0.560

calculated at the M062X/6-311++G(d,p) level and represented in Fig. 9.

Different values of electrostatic potential at MEP map are shown by different colors, which are between red and blue. The color between red and green in MEP map are related to electrophilic reactivity, the color between green and blue in MEP map is related to nucleophilic reactivity. According to Fig. 9, electrophilic active regions are around the S atom in TH and N1, O1 and O2 atoms in TBA molecule. As for the MEP contour, yellow lines are related to positive charge while red lines are related to negative charges [38]. According to MEP contours, steric effects around N2 atom in TBA are seen clearly, and S atom is an active site for TH while N1 atom is mainly an active site for TBA molecule.

3.2.4 Solvent Effect

Electrochemical reactions take place in solution, and it is important to take into account the solvent effects when TH is dyeing the interaction between metal and inhibitors. It is known that the phenomenon of electrochemical corrosion appears mainly in water, and it is expected that the inhibiting molecules in solution behave differently from that in gas phase. It is therefore, necessary to include the solvent effect in the computations. Investigated inhibitors are re-optimized at M062X/6-311++G(d,p) level in water. Mentioned descriptors are recalculated and listed in Table 4.

According to above explanation, as in "Non-protonated inhibitor" section, inhibition efficiency ranking is calculated mainly as follows, except nucleophilicity index:

TH > TBA

3.3 Surface Analysis

The AFM technique was employed to reveal the surface microstructure of metal after the corrosion test [39]. Figure 10 depicts the morphologies of steel specimens

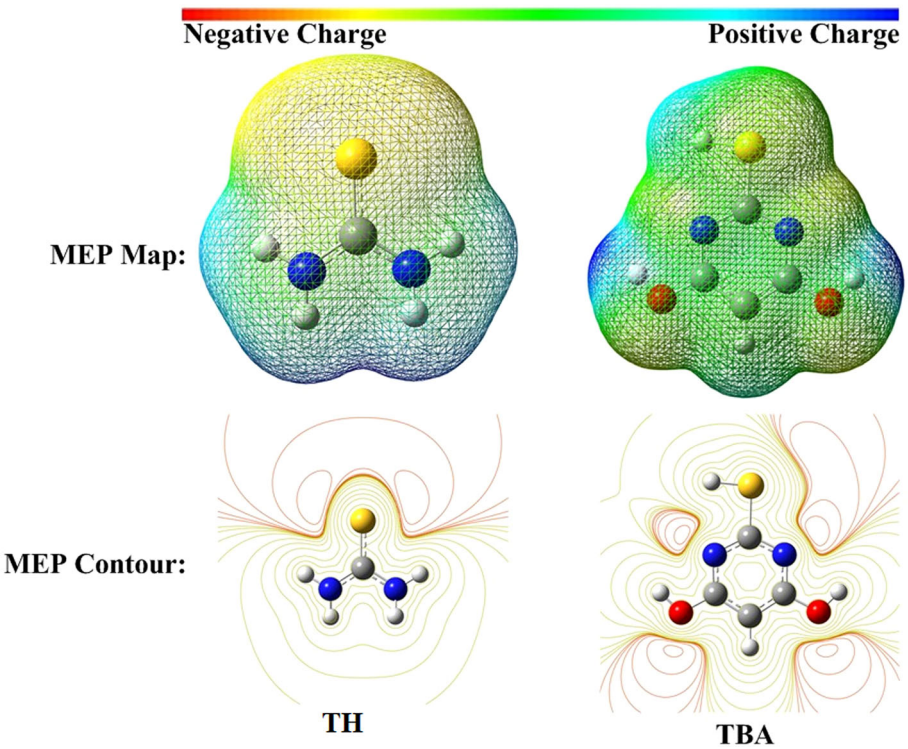

Fig. 9 MEP maps contours of investigated inhibitors at M062X/6-311++G(d,p) level in gas phase

Table 4 Quantum chemical descriptors for non-protonated inhibitors at M062X/6-311++G(d,p) level in water

Inhibitor	E_{HOMO} (eV)	E_{LUMO} (eV)	E_{GAP} (eV)	I (eV)	A (eV)
TU	−7.745	−0.005	7.740	1.590	6.236
TBA	−9.519	1.271	10.790	0.807	6.957
Inhibitor	η (eV)	σ (eV^{-1})	χ (eV)	ω (eV)	N (eV^{-1})
TU	2.323	0.430	3.875	3.232	0.309
TBA	3.075	0.325	4.124	2.766	0.362

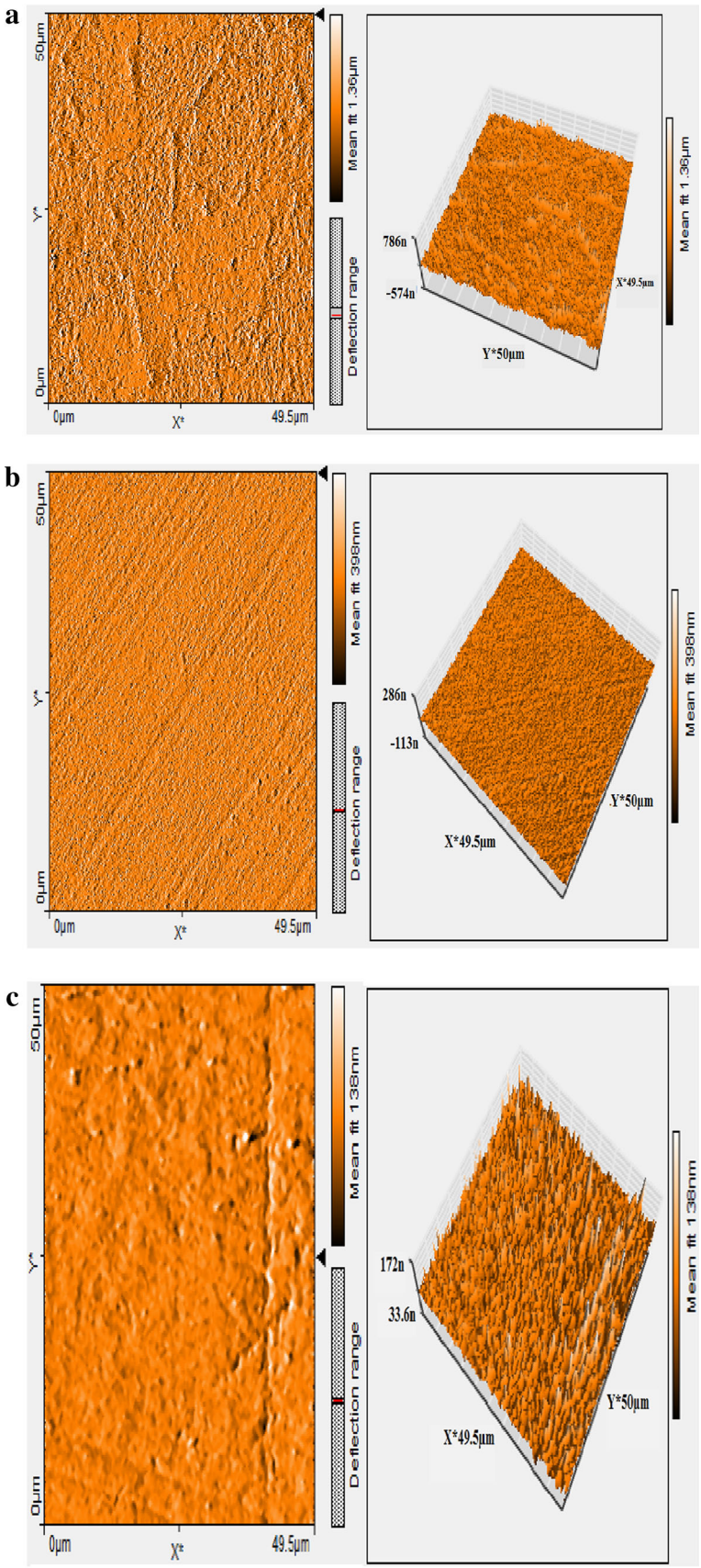

Fig. 10 Surface of steel electrode by atomic force microscopy after 6 h immersion at OCP in 1 M HCl solution: **a** without **b** with 6×10^{-3} M TBA and **c** with 6×10^{-3} M TH

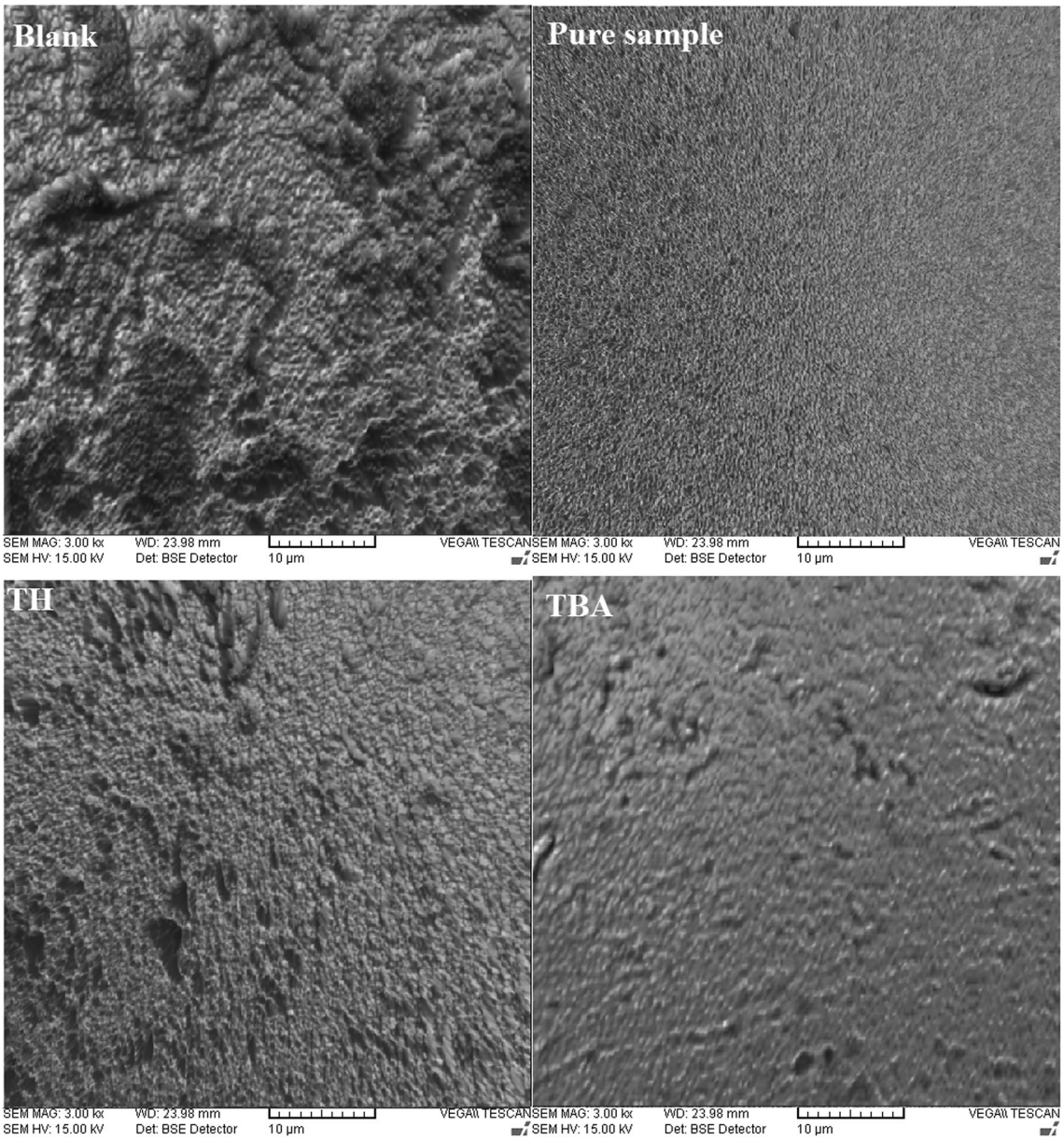

Fig. 11 Surface of steel electrode by SEM micrograph after 6 h immersion at OCP in 1 M HCl solution: **a** without **b** with 6×10^{-3} M TBA and **c** with 6×10^{-3} M TH

after immersion for 6 h in 1 M HCl solutions without and with 6×10^{-3} M TH and TBA. In the absence of inhibitor (Fig. 10a) the surface displayed a very irregular topography due to corrosion attack. The average roughness R_a of steel in 1 M HCl solution without inhibitor was calculated as 1.36 µm by atomic force microscopy (Fig. 10a). In the presence of TH and TBA, smoother surface was obtained and the R_a value decreased to 138 and 396 nm (Fig. 10b, c) as a consequence of low corrosion damage and the protective formation of an inhibitor layer on the steel surface.

Figure 11 represents the micrograph obtained for steel samples in presence and in absence of 6×10^{-3} M inhibitors after immersion for 6 h. It is clearly seen that steel surfaces suffer from severe corrosion attack in the blank sample. It is important to stress out that when the compound is present in the solution, the morphology of steel surface is quite different from the previous one, and the specimen surfaces were smoother. We noted the formation of a film which is distributed in a random way on the whole surface of the steel. This may be interpreted as due to the adsorption of the inhibitors on the steel surface incorporating into the

passive film in order to block the active site present on the steel surface. Alternatively, the involvement of inhibitor molecules in the interaction with the reaction sites of steel surface, resulted in a decrease in the contact between steel and the aggressive medium and sequentially exhibited excellent inhibition effect [40, 41].

4 Conclusions

The following main conclusions are drawn from the present study:

1. The addition of TH and TBA compounds to the 1 M HCl solution reduces corrosion of steel. It was found that TH is more efficient corrosion inhibitor for steel protection.
2. Polarization measurements demonstrate that inhibitors behaved as mixed type corrosion inhibitor by inhibiting both anodic metal dissolution and cathodic hydrogen evolution reactions.
3. Impedance measurements indicate that with increasing inhibitor concentration, the polarization resistance (R_{ct}) increased, while the double-layer capacitance (C_{dl}) decreased.
4. The high resolution AFM and SEM micrographs were shown. The corrosion of steel in 1 M HCl solution was described by corrosion attack and the addition of inhibitors to the aggressive solutions diminished the corrosion of steel.
5. Data was obtained from quantum chemical calculations at M062X/6-311++G(d,p) level in gas phase. Levels of theory were correlated to the inhibitive effect of inhibitors. Both experimental and theoretical calculations are in agreement. Theoretically, inhibition efficiency ranking mainly is determined as TH > TBA.

Acknowledgments The authors wish to acknowledge the financial support of the Office of Vice Chancellor of Research of their corresponding universities. We are grateful to the office of scientific research projects of Cumhuriyet University (Project No.: F-372) for financial supports. The numerical calculations reported in this paper are performed at TUBITAK ULAKBIM, High Performance and Grid Computing Center (TRUBA Resources).

References

1. Fouda A S, Mostafa H A, Heakal F E, and Elewady G Y, *Corros Sci* **47** (2005) 1988.
2. Yurchenko R, Pogrebova L, Pilipenko T, and Shubina T, *Russ J Appl Chem* **79** (2006) 1100.
3. Jafari H, Danaee I, Eskandari H, and RashvandAvei M, *J Mater Sci Technol* **30** (2014) 239.
4. Sastri V S, Green Corrosion Inhibitors-Theory and Practice, John Wiley & Sons, Inc., Hoboken (2011).
5. Jafari H, Danaee I, Eskandari H, and RashvandAvei M, *J Environ Sci Health Part A* **48** (2013) 1628.
6. Turnbull A, Coleman D, Griffiths A J, Francis P E, and Orkney L, *Corrosion* **59** (2003) 250.
7. Jafari H, Akbarzade K, and Danaee I, *Arab J Chem* (2014). doi: 10.1016/j.arabjc.2014.11.018.
8. Bentiss F, Bouanis M, Mernari B, Traisnel M, Vezin H, and Lagrenee M, *Appl Surf Sci* **253** (2007) 3696.
9. Stanly Jacob K, and Parameswarn G, *Corros Sci* **52** (2010) 224.
10. Lowmunkhong P, Ungthararak D, and Sutthivaiyakit P, *Corros Sci* **52** (2010) 30.
11. Ghareba,S and Omanovic S, *Electrochim Acta* **56** (2011) 3890.
12. Hua X, Alzawaia K, Gnanavelua A, Nevillea A, Wang C, Crossland A, and Martin J, *Wear* **271** (2011) 1432.
13. Morales-Gila P, Negro-Silva G, Romero-Romo M, Ángeles-Chavezc C A, and Palomar-Pardave M, *Electrochim Acta* **49** (2004) 4733.
14. Eliyan F F, Mahdi E, and Alfantazi A, *Corros Sci* **58** (2012) 181.
15. Tang F, Wang X, Xu X, and Li L, *Colloids Surf A* **369** (2010) 101.
16. Godec R F, and Dolecek V, *Colloids Surf A* **244** (2004) 73.
17. Negm N A, Ghuiba F M, and Tawfik S M, *Corros Sci* **53** (2011) 3566.
18. Ozcan M, and Dehri I, *Progr Organ Coatings* **51** (2004) 181.
19. Saxena N, Kumar S, Sharma M K, and Mathur S P, *Pol J Chem Technol* **15** (2013) 61.
20. GaussView, Version 5, Roy Dennington, Todd Keith, and John Millam, Semichem Inc., Shawnee Mission (2009).
21. Gaussian 09, Revision C.01, Frisch M J, Trucks G W, Schlegel H B, Scuseria G B, Robb M A, Cheeseman J R, Scalmani G, Barone V, Mennucci B, Petersson G A, Nakatsuji H, Caricato M, Li X, Hratchian H P, Izmaylov A F, Bloino J, Zheng G, Sonnenberg J L, Hada M, Ehara M, Toyota K, Fukuda R, Hasegawa J, Ishida M, Nakajima T, Honda Y, Kitao O, Nakai H, Vreven T, Montgomery J A, Jr., Peralta J E, Ogliaro F, Bearpark M, Heyd J J, Brothers E, Kudin K N, Staroverov V N, Kobayashi R, Normand J, Raghavachari K, Rendell A, Burant J C, Iyengar S S, Tomasi J, Cossi M, Rega N, Millam J M, Klene M, Knox J E, Cross J B, Bakken V, Adamo C, Jaramillo J, Gomperts R, Stratmann R E, Yazyev O, Austin A J, Cammi R, Pomelli C, Ochterski J W, Martin R L, Morokuma K, Zakrzewski V G, Voth G A, Salvador P, Dannenberg J J, Dapprich S, Daniels A D, Farkas Ö, Foresman J B, Ortiz J V, Cioslowski J, and D. J. Fox, Gaussian, Inc., Wallingford (2009).
22. Perkin Elmer, ChemBioDraw Ultra Version (13.0.0.3015), Cambridge Soft Waltham, Waltham (2012).
23. Zhao Y, and Truhlar D G, *Theor Chem Acc* **120** (2008) 215.
24. Yıldız R, *Corros Sci* **90** (2015) 544.
25. Zhang K, Xu B, Yang W, Yin X, Liu Y, and Chen Y, *Corros Sci* **90** (2015) 284.
26. Guo L, Zhu S, Zhang S, He Q, and Li W, *Corros Sci* **87** (2014) 366.
27. Doğru Mert B, Ongun Yüce A, Kardas G, and Yazıcı B, *Corros Sci* **85** (2014) 287.
28. Obot I B, and Gasem Z M, *Corros Sci* **83** (2014) 359.
29. Sayin K, and Karakaş D, *Corros Sci* **77** (2013) 37.
30. Karakus N, and Sayin K, *J Taiwan Inst Chem Eng* **48** (2015) 95.
31. Erkan Kariper S, Sayın K, Karakaş D, *Hacettepe J Biol Chem* **42** (2014) 337.
32. Abboud Y, Abourriche A, Saffaj T, Berrada M, Charrouf M, Bennamara A, Hannache H, *Desalination* **237** (2009) 175.
33. Ashassi-Sorkhabi H, Shaabani B, Seifzadeh D, *Appl Surf Sci* **239** (2005) 154.
34. Chetouani A, Hammouti B, Benhadda T, and Daoudi M, *Appl Surf Sci* **249** (2005) 375.
35. Jafari H, Danaee I, Eskandari H, RashvandAvei M, *Ind Eng Chem Res* **52** (2013) 6617.

36. Emregül K C, and Atakol O, *Mat Chem Phys* **82** (2003) 188.
37. Fujioka E, Nishihara H, and Aramaki K, *Corros Sci* **38** (1996) 1915.
38. Govindasamy P, and Gunasekaran S, *Spectrochim Acta Part A* **136** (2015) 1543.
39. Prabhu R A, Venkatesha T V, Shanbhag A V, Kulkarni G M, and Kalkhambkar R G, *Corros Sci* **50** (2008) 3356.
40. Moretti G, Quartanone G, Tassan A, and Zingales A, *Wekst Korros* **45** (1994) 641.
41. Gewirth A, and Niece B K, *Chem Rev* **97** (1997) 1129.